Exp. Theo. NANOTECHNOLOGY 10 (2026) 25-36 https://doi.org/10.56053/10.1.25

Structural and photocatalytic insights into anatase TiO_2 nanostructure for dye degradation

Ali Q. Tuama[1], *Ghaiath A. Fadhil*[1,2,*], *Wael A. S. Al-dulaimi*[1]

[1]College of Science, Al-Karkh University of Science, Baghdad, Iraq
[2]College of Engineering, Al-Karkh University of Science, Baghdad, Iraq
[*]) Email: ghaiath.fadhil@kus.edu.iq

Received 22/9/2025, *Received in revised form* 25/11/2025, *Accepted* 3/12/2025, *Published* 15/1/2026

TiO_2 nanostructures are synthesized through Sol-gel method using titanium tetracypropoxide (TTIP) as the precursor. Acetic acid is used as chelating and peptizing agent and the deionized water as a solvent the prepared gels are deposited on glass substrates through dip-coating and subjected to controlled temperatures calcinations. X-ray diffraction (XRD) and field emission scanning electron microscopy (SEM) are used to characterize the obtained materials structurally morphologically. The findings indicated the dominance of the anatase phase with crystallites sizes of nanometers. Although SEM analysis showed a network such as a nanostructure of the particles that are less than 100 nm. To assess the possible environment application. Photocatalytic activity of the synthesized TiO 2 films is studied by observing the decomposition of the methylene blue (MB) dye under Uv. The findings had shown that the Sol-gel prepared TiO_2 displays good photocatalytic behavior. Where the calcine sample had a dye degradation greater than 80% with the reaction time of 120 minutes. The increased performance is due to better crystallinity and preponderance of anatase phase as compared to lower activity in the non-calcine sample. This observation proves the point. Therefore, Sol gel approach is a simple and effective route to the production of TiO_2 nanostructures, which can be used in the purification of wastewater.

Keywords: Titanium dioxide; Sol–gel; Nanostructures; Photocatalysis; Methylene blue.

1. INTRODUCTION

Titanium dioxide titanium (TiO_2) is one of the broadly studied metal oxide semiconductor due to its varied physical chemical. And functionality that enables it to be used in many scientific and industrial uses, [1-4] due to its large bandgap, (about 3.2 eV) in the case of anatase phase. High chemical stability, non-toxicity and high photocatalytic performance. There are various applications of (TiO_2) in various

areas which include photocatalysis, photovoltaics, energy conversion, gas sensing and so on. And biomedical devices [1-4]. The crystalline structure of (TiO_2) consists of three phases anatase, rutile and bruchite. Anatase structure is the most active in terms of photocatalysis because it is highly reactive on the surface and the separation of charge carriers is effective [5]. It is necessary to control morphology and crystallinity of (TiO_2) nanostructures to enhance their usage in numerous technological processes. An example is high surface area morphology like nanotubes, nanofibers, nanowires and porous films that offer increased active sites to interfacial reactions and the control of the phase composition ratio (anatase/ rutile) that controls the. Electron hole processes and consequently photocatalytic performance [6-7].

These structural and morphological optimizations have been reported using different methods of synthesis including hydrothermal growth, Sol-gel chemistry, phase deposition. And electrochemical anodization [8-11]. Mosto of these reports focused on powders but not thin films. The Sol-gel method is one of the existing methods of fabrication, and it is known as a simple and cost-effective procedure that enables one to create TiO_2 nanostructures in uniform composition and adjustable morphology. In specific vapor phase control in the case of mild synthesis [12,13]. The Sol-gel process entails hydrolysis and condensation reaction of titanium alkoxides, EEG, titanium tetracypropoxide, TTIP, gelation, drying and calcination. The stability of the Sal is improved by the presence of chelating agents like acetic acid that ensures the avoidance of uncontrolled precipitation resulting in uniform nanoparticles in films [14]. Additionally, TiO_2 coatings prepared with Sol gel by the use of the dip coating or spin coating are characterized by reproducible thickness control, high optical transparency, and a high substrate adhesion. [15].

The pertinence of the photocatalytic research has now shifted to the manner of environmental remediation due to the increased dumping of organic dyes and dangerous pollutants to the water body through the textile industry. Leather, Pharmaceutical, [16,17], Some of the type organic dyes. Methylene blue MB is extensively used to determine the Photocatalytic activity of TiO_2 materials. Because of its stability, defined absorption spectrum and environmental relevance [18]. TiO_2photocatalysts can be stimulated by UV radiation to produce reactive oxygen species Ros, including hydroxyl radicals and superoxide anions. Which is capable of breaking down MB molecules into less toxic byproducts [19]. It has been extensively established that the synthetic conditions especially the calcification temperature and time primarily influence the photocatalytic activity of Sol gel derived TiO_2 as they dominate the transformation of the anatase to the rutile crystal [20 -22]. It has been revealed that in the past the Sol gel TiO_2 balcony has been able to attain almost 100% destruction of MB in (2-4) hours under UV light. On re-usage with better reusability if good calcinations are applied [23]. These reports focused on degradation effieciency. More interest should be given to linking the structure to phase growth. Moreover, Dr surface modified TiO_2 system has been reported to be extended to the visible region with pure anatase TiO_2 [24].

Although the use of hydrothermal routes has been improved greatly, it still has limitations in scalability. In our laboratory, our previous study showed good hydrothermal growth and characterization of TiO_2 nanotubes and nanofibers [25]. The nanotubes of titania are prepared through a specially designed hydrothermal system and structural and morphological properties of the system are analysed by the use of XRD and SEM [25]. Moreover, TiO_2 nanofibers are made and tested against bacterial and fungal selectivity. The disclosure of the potential antifungal efficacy against Candidiasis [26] has relegated a strong ground of the current research, based on previous hydrothermal techniques, through the usage of the Sol gel method as an easy and scalable alternative.

The aim of the present research is (*i*) to prepare TiO_2 nanostructures through the Sol-gel process by using TTIP as starting material and acetic acid as the chelating agent and (*ii*) to test their ability to catalyse methylene. Temperatures 400 and 550 °C are selected to compare anatase phase dominance at lower

temperature with a higher temperature where the transformation to rutile may begin. In the structural and morphological study, (Figure 1), the XRD and SEM methods are used to analyse the structural and morphological characteristics of the systems and the photocatalytic activities of the particles under the UV irradiation conditions. The synthesis of the study by combining the structural analysis with the applications in the environmental context gives new knowledge concerning the correlation between the synthesis parameters. Crystallinity Morphology. And photocatalytic performance of Sol-gel obtained TiO_2 nanostructures.

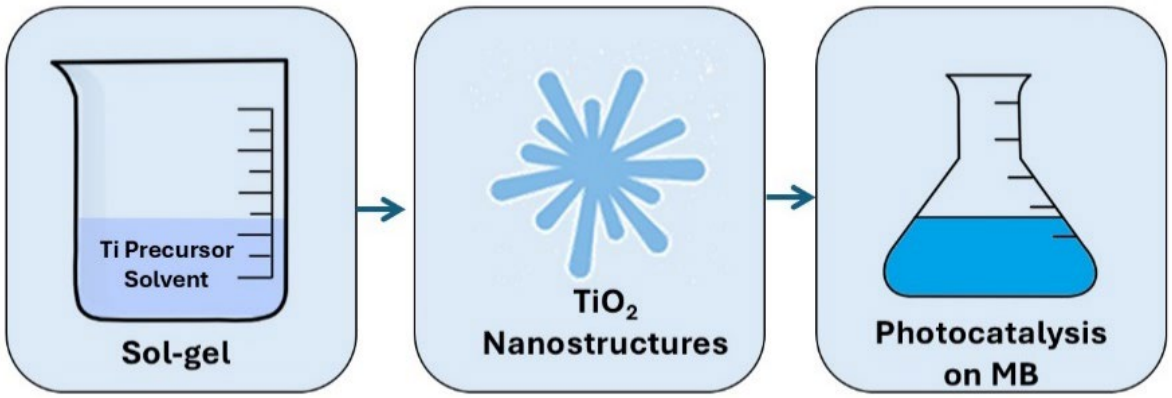

Figure 1 Schematic illustration of the sol–gel synthesis of TiO_2 nanostructures and their photocatalytic application in methylene blue degradation.

2. EXPERIMENTAL

2.1 Materials

Titanium tetracypropoxide, TTIP 97%, glacial acetic acid, CH_3COOH, 99% in deionized water are utilized as precursors in this work. TTIP is supplied by Sigma-Aldrich. All reagents are of analytical grade and employed without additional purification. Glass slides served as substrates for the coating of TiO_2 films.

2.2 Synthesis of TiO_2 Nanostructures (Sol–Gel Method)

The TiO_2 nanostructures are obtained using a conventional Sol-gel route. In a typical process, TTIP is added dropwise into a premixed solution of glacial acetic acid and deionized water while maintaining constant magnetic stirring at ambient temperature for 60 minutes. A molar proportion of TTIP AcOH:H_2O equal to 1:4:20 is selected to promote a uniform hydrolysis condensation reaction. The resulting clear saw is left to age for 24-H to improve its homogeneity and stability. Subsequently the Sol is deposited onto pre cleaned glass substrates by the dip coating technique with a speed of withdrawal of 5 cm/min for 3 coating cycles and dried at 100°C for 2H. The resulting zero goals are then treated in air at 400 °C sample A and 550 °C sample B for 2H with a heating rate of 5 °C/min to obtain crystalline TiO_2 films. The temperature of 400 °C is selected because TiO_2 normally shows mainly anatase phase at this value, while 550 °C is selected to examine the effect of higher temperature on growth of rutile phase. This helps to understand the influence of thermal treatment on photocatalytic behaviour.

2.3 Characterization

The crystalline phases of the obtained TiO_2 samples are examined by X-ray diffraction. Xard CU Kα, λ = 1.5406 Å within a 2θ scanning range of 10° to 80° with a step size of 0.02°. Average crystallite

dimensions are estimated through the sharer relationship considering the 101 diffractions of anatase. The morphology and particle arrangement are investigated using field emission scanning electron microscopy. FESCM Inspect. F50 FAE operating AT 30KV. Images are recorded under multiple magnifications to assess the surface texture and nanostructural evolution.

The photocatalytic activity of the Sol gel derived TiO_2 films is tested through the degradation of methylene blue MB used as a representative organic contaminant. Each experiment employed 100 milliliters of a 10 milligrams LMB solution. Before exposure, the mixture containing the TiO_2 film is magnetically stirred in darkness for 30 minutes to establish adsorption desorption equilibrium. The distance between the UV source and the reactor is fixed at 10 cm. Photocatalytic reactions are then conducted under UV illumination (365 nm, 15 W) at ambient temperature. Samples of the solution are collected at specific intervals 3060, ninety, 120 and 180 minutes. And the residual MB concentration is analyzed by UV vis spectrophotometry at 664 nanometers. UV analysis is used because pure TiO_2 is mainly active under ultraviolet irradiation. The photocatalytic efficiency is calculated according to.

$$\text{Degradation efficiency } (\%) = \left(\frac{1-C_t}{C_0}\right) 100\% \quad (1)$$

where C_0 is initial concentration of MB, and C_t is concentration at time t.

3. RESULTS AND DISCUSSION

The phase evolution and crystallinity of the Sol gel derived TiO_2 nanostructures are examined by X-ray diffraction XRD. The diffraction profile of the Uncalcin sample, Sample A in Figure 2 exhibited broad and weak reflections, confirming its largely amorphous nature. The lack of distinct Anita's peaks suggests that heat treatment is required to induce crystallization. After calcination at 400°C, sample B in Figure 2 The diffraction pattern exhibited clear and intense peaks located at 2θ = 25.3° (101), 37.8°, (004) 48.0°, (200) 53.9°, (105) and 62.7° (204). Corresponding to the anatase phase of titanium 4 oxide. JCPDS 21 -, 1272. The sharpness and reduced FWHM of these peaks demonstrate the emergence of well crystallized anatase nanostructures. When the calcination temperature increased to 550 °C, sample C in Figure2 an additional reflection appeared at 27.4° corresponding to the rutile 110 plane. JCPDS 21 -, 1276. This observation indicates the initial formation of the rutile phase and the beginning of the anatase to rutile conversion process, which is thermodynamically promoted at elevated temperatures. Despite this transition, Annette's remained the predominant phase, while rutile existed as a minor component. The average crystallite size of TiO_2 nanoparticles is estimated using the Scherer equation.

$$D = \frac{K\lambda}{\beta cos\theta} \quad (2)$$

where K is the shape factor (0.9), λ is the CUK αwavelength (1.5406. Å) β is the full width at half maximum. (FWHM) of the main diffraction peak in radians and θ as the Bragg angle. Table 1 lists the estimated crystallite sizes. No size could be determined for the uncalcined sample because of its amorphous nature. Whereas the samples calcined at 400°C and 550°C showed average crystallite sizes of around 21 nm and 34 nm respectively. The growth in particle size with temperature is mainly associated with grain coarsening and partial phase transformation.

Table 1 Average crystallite size of TiO_2 nanostructures calculated from the (101) anatase peak using Scherrer equation.

Sample	Main Phase	2θ (°)	FWHM (rad)	Crystallite Size (nm)
A (As-prepared)	Amorphous/Weak Anatase	broad hump	–	–
B (400 °C)	Anatase	25.3 (101)	0.0072	21.5
C (550 °C)	Anatase + Rutile	25.3 (101), 27.4 (110)	0.0045	34.2

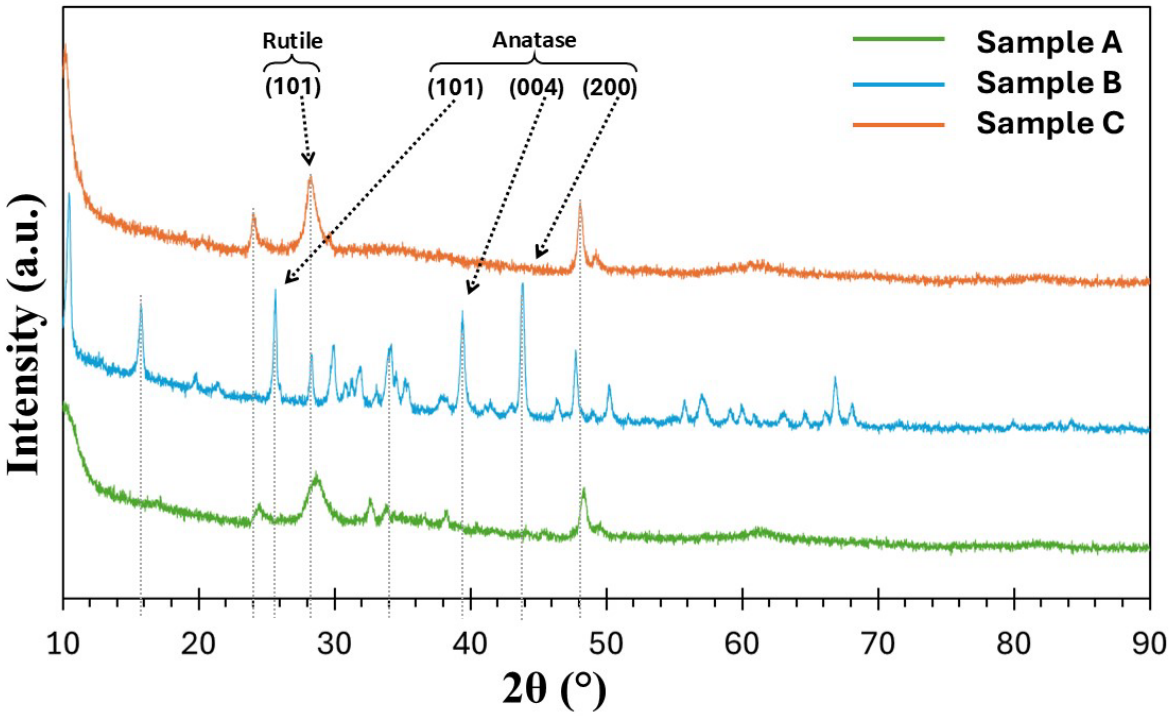

Figure 2 XRD pattern of TiO_2 nanostructures for the as-prepared state (sample A), calcination at 400 °C (sample B) and calcination at 550 °C (sample C).

The surface morphology of the as prepared TiO_2 nanoparticles, (Figure 3a) reveals that the powder exhibits a compact network of irregular clusters and a sponge like morphology. This is showing minimal crystal in order. This observation is consistent with the amorphous weak annatase phase identified in the XRD pattern. At higher magnification, (Figure 3b), the surface appears rough and featureless without clear particle boundaries, further confirming the amorphous nature of the as prepared sample. Such morphology is typical for TiO_2 prepared by Sol-gel methods prior to calcination, where the particles are poorly crystallized and strongly interconnected. These images show irregular agglomerated structures without well-defined particle boundaries. The apparent agglomerate size is estimated to range between 80–150 nm, which is consistent with the amorphous nature of the uncalcined sample.

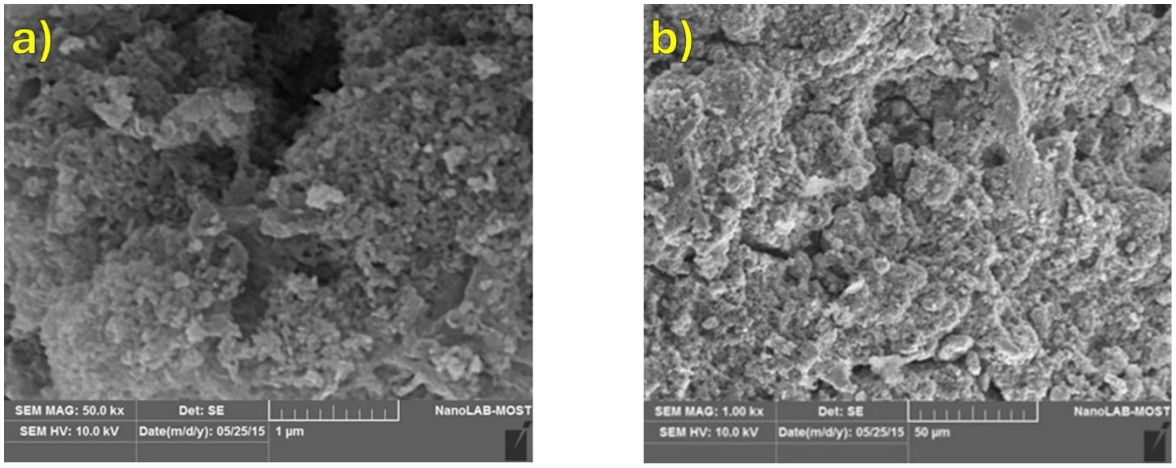

Figure 3 SEM images of the as-prepared TiO_2 nanoparticles: (a) low magnification and (b) high magnification.

Figure 4 depicts the morphology of TiO_2 nanoparticles that have been sintered at 400 °C. At this temperature, the particles begin to crystallize to produce well defined nanostructures which are relatively uniformly dispersed. As seen in Figure 4A. Nanoparticles on the surface are interlocked with greater crystallinity as compared to the as made state. Figure 4B here is a magnified view of the particles with a size of predominately 20 -30 nm with an occasional large aggregate of up to ~150 nm. The results indicate that anatase is preferentially formed at heating temperatures of 400 °C. Nanocrystals in good concord with the XRD. Such morphology provides a larger surface to volume ratio, which is preferable to modify the photocatalytic activity.

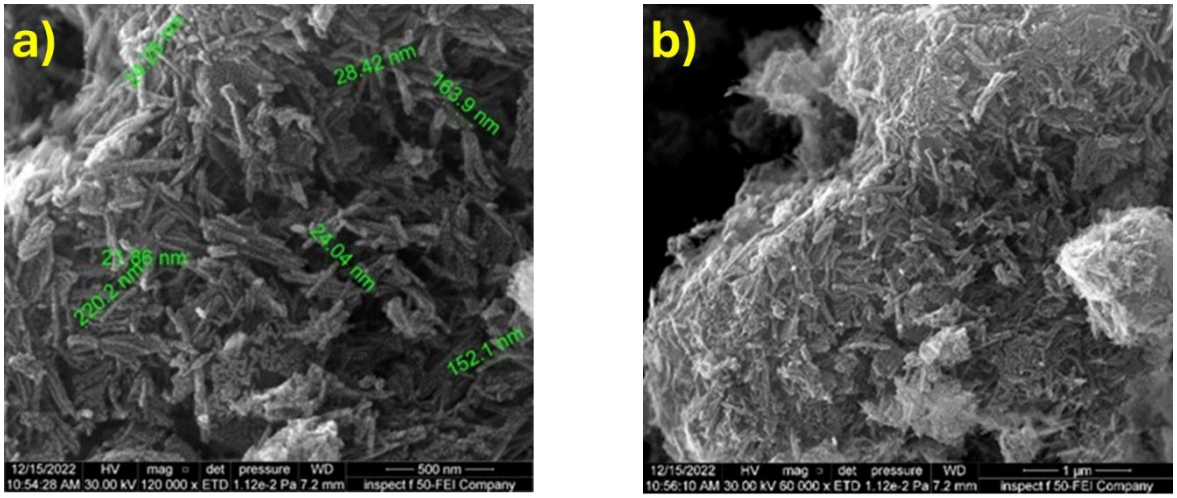

Figure 4 SEM images of TiO_2 nanoparticles calcined at 400 °C: (a) low magnification and (b) higher magnification.

The morphology of TiO_2 nanoparticles calcined at 550 °C is shown in Figure 5. At this temperature, the nanoparticles undergo significant grain growth. Forming the elongated rod-like structures that are clearly distinguishable in the high magnification image (Figure 5a). The surface becomes denser and less porous compared to the 400°C sample. Which is also confirmed by the lower magnification view (Figure 5b) showing aggregated nanorods with reduced interparticle voids. These morphological changes suggest that increasing the calcination temperature promotes crystallite growth and structural densification. These images clearly reveal elongated nanorod-like structures. The nanorods possess estimated diameters of 40–60 nm and lengths ranging from 200–300 nm. In line with the XRD results that revealed the coexistence of anatase and rutile phases. Such transformation is expected to influence the optical and photocatalytic properties of TiO_2 due to the reduced surface area and increased crystallinity.

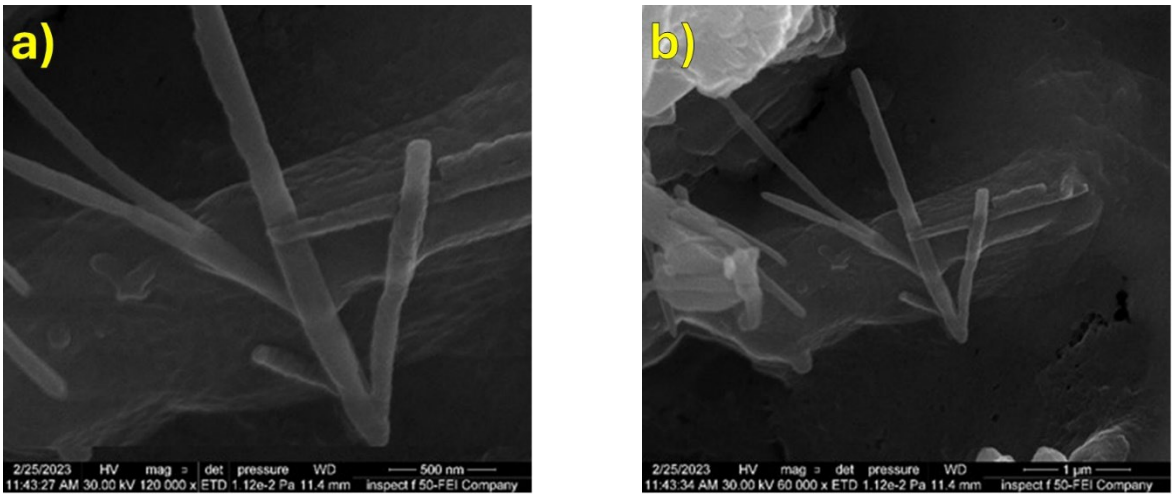

Figure 5 SEM images of TiO_2 nanoparticles calcined at 550 °C: (a) high magnification image and (b) lower.

The SEM images revealed a larger grain size. The as-prepared sample has amorphous agglomerates without defined crystallites. The sample calcined at 400 °C exhibits nanorods with diameters of the particles with a size of predominately 20 -30 nm while the sample calcined at 550 °C exhibits nanorods with diameters of 40–60 nm. Compared to XRD crystallite size, SEM revealed a larger grain size. This is expected since each SEM-visible grain typically consists of multiple coherent crystallites. The photocatalytic performance of the Sol-gel synthesized TiO_2 films is tested by observing UV-induced decomposition of methylene blue MB dye. Before illumination, the suspension containing the TiO_2 samples is kept under magnetic stirring in the dark for 30 minutes to reach adsorption desorption balance. Variations in MB concentration during exposure are recorded using a UV Vis spectrophotometer at 664 nm.

The degradation efficiency is calculated using equation one mentioned above. Figure 6 shows the photo catalytic degradation curves of MB for the three samples as prepared, a 400 °C sample B and 550 °C sample C. Be as prepared. Sample exhibited very low photocatalytic activity due to its amorphous structure and limited surface area. In contrast, the sample calcined at 400°C demonstrated the highest degradation efficiency, achieving ~90% removal of MB within 180 minutes. This superior activity can be attributed to the well-defined anatase nanostructures, high surface area and reduced recombination of photogenerated charge carriers. The sample treated at 550 °C shows moderate photocatalytic activity compared to the 400 °C sample. This can be related to grain coarsening and the anatase to rutile transformation. It indicates that unnecessary calcination temperature can reduce the photocatalytic efficiency.

For the sample calcined at 550 °C. The degradation efficiency decreased compared to the 400 °C sample, reaching ~70% after 180 minutes (Table 2). The reduced performance is related to the grain growth, reduced surface area. And partial anatase to rutile transformation, which decreases the density of active sites but improves crystallinity. The balance between these factors explains the moderate photocatalytic performance.

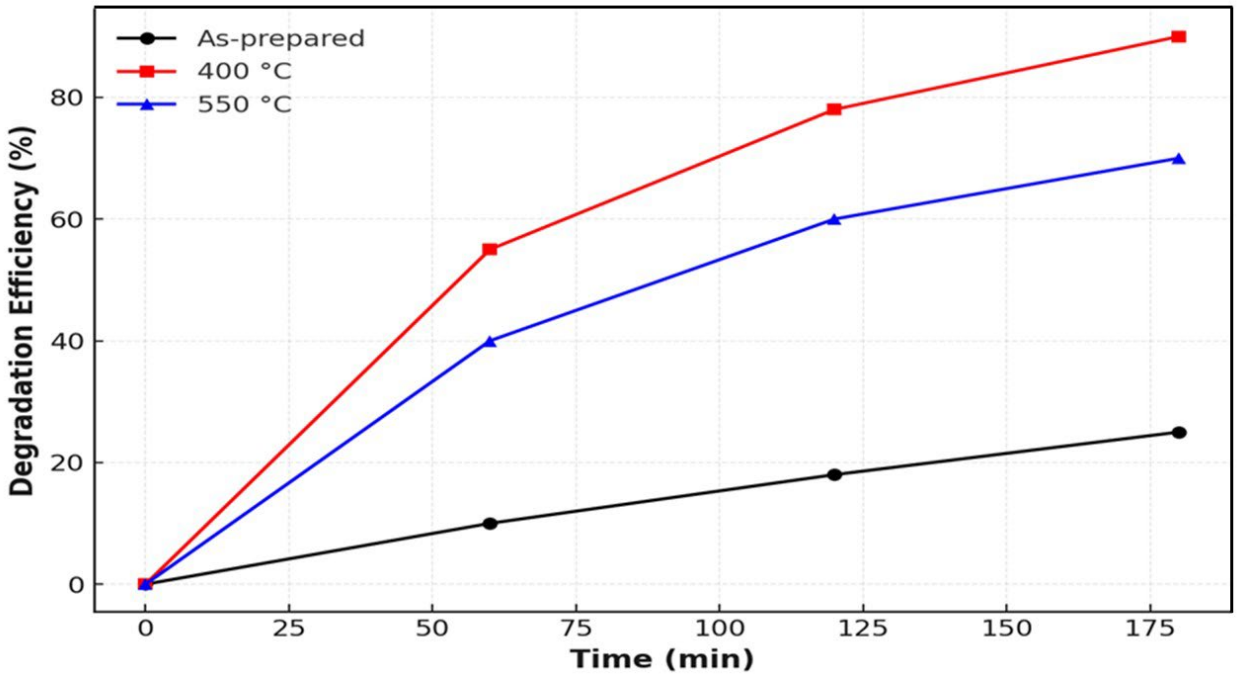

Figure 6 Photocatalytic degradation of methylene blue (MB) under UV irradiation using TiO_2 nanostructures.

Table 2 Degradation efficiency at different times.

Sample	60 min	120 min	180 min	Efficiency (%)
As-prepared	10	18	25	Low
400 °C	55	78	90	High
550 °C	40	60	70	Moderate

The results show that photocatalytic performance of TiO_2 nanostructures is strongly dependent on their crystalline phase, particle size, surface area, and morphology (Figure2). The as prepared sample exhibited an amorphous structure which limited its photocatalytic activity. Figure 6. Amorphous TiO_2 contains a high density of structural defects and lacks long-range order. Leading to high recombination rates of photogenerated electron hole (e^-/h^+) pairs. Consequently, only a small fraction of charge carriers contributes to the formation of reactive oxygen species Ros. at 400°C the material is predominantly composed of well crystallized anatase nanoparticles with high surface to volume ratio. (Figures 2 and 4). Anatase is well known for its superior photocatalytic properties due to its suitable bandgap, (~3.2 eV), low recombination rate of VH pairs and strong ability to absorb organic molecules. The porous nanostructure at this stage provided abundant active sites for dye adsorption and roast generation, resulting in the highest degradation efficiency, ~90%.

When the calcination temperature increased to 550 °C, the growth of larger nanocrystals in the onset of anatase to rutile transformation are observed. (Figures 2 and 5). Although rutile has a narrower band gap, (~3.0 eV), which allows better light absorption. It's higher recombination rate and lower surface area reduced the overall photocatalytic performance compared to the 400 °C sample. However, the coexistence of anatase and rutile phases can create heterojunctions that facilitate charge separation,

partially enhancing photocatalytic stability. This explains why the 550 °C sample still exhibited moderate activity, ~70%.

The photocatalytic behavior of TiO_2 under ultraviolet exposure is depicted in Figure 7. When you radiated with photons possessing energy equal to or higher than its band gap TiO_2 becomes photoexcited, producing electron hole pairs. The excited electrons transition to the conduction band CB, while the corresponding holes remain localized in the valence band. These charge carriers drive a sequence of redox reactions involving surface adsorbed species. Electrons interact with dissolved oxygen to yield superoxide radicals. ($\bullet O_2^-$). Whereas holes oxidize surface hydroxyls and water molecules generating hydroxyl radicals. (•OH). The reactive oxygen species produced in this process play the key role in decomposing methylene blue MB into environmentally benign products such as CO_2 and H_2O. This mechanism explains the higher degradation efficiency observed for the calcined TiO_2 samples, especially at 400 °C, where better crystallinity enhances charge separation. It also supports the experimental trends shown in Figure 6.

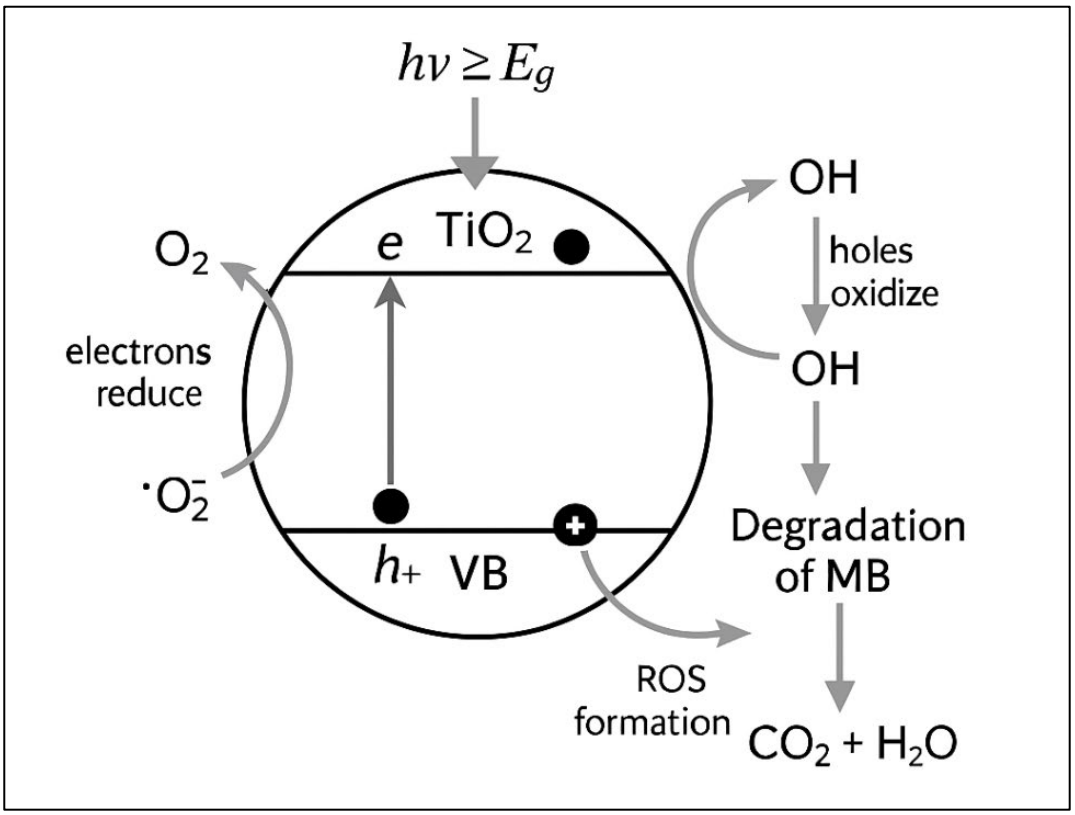

Figure 7 Schematic representation of photocatalytic mechanism of TiO_2 nanostructures under UV irradiation [6].

4. CONCLUSIONS

In this study, TiO_2 thin films were prepared by the sol–gel method and deposited on glass substrates by dip coating. TiO_2 nanostructures were prepared through a relatively simple Sol-gel roof that was subsequently analyzed systematically in regard to their structural, morphological and photocatalytic characteristics. The XRD pattern has been used to establish that the uncalcinated substance had an amorphous phase of the substance that was subjected to heating to 400 °C and the resulting crystalline

anatase. And further warming to 550 °C commenced a small fraction of conversion to rutile. This confirms the dominance of the anatase phase as also stated in the abstract. In the case of the SCM observations, it was observed that the surface texture of a normal clusters changed before the transformation of the calcification to interconnected nanoparticles at 400 °C and in the elongated grains at 550 °C. The observed particle size remained within the nanometer scale and mostly below 100 nm. The experiments on photocatalysis of methylene blue MB under the UV light were conducted to demonstrate that the most active sample was the sample that was treated at 400 °C because it degraded nearly 90 percent of the MB in 180 minutes. This improvement is mostly related with fine crystallinity and the existence of more surface area of anatase phase that contributed to the charge separation and provision of multiple areas of activity of the reaction. Conversely, the least active sample was the unheated sample due to the amorphous structure, the sample heated to 550 °C due to coarse grains and part of anatase converting to rutile. This last finding further elucidates that the temperature of the calcification is a determining factor in regards to the Crystallinity and the photocatalytic characteristics of TiO_2 materials synthesized by the Sol-gel method. The optimized sample that has undergone optimization at 400 °C is a good indication of the viable environmental cleanup in the real sense particularly in the wastewater purification systems. Therefore, the prepared TiO_2 films show good potential for wastewater purification applications.

References

[1] Chen Xiaobo, Samuel S. Mao, Chemical reviews 107.7 (2007) 2891 https://doi.org/10.1021/cr0500535
[2] Prashant V Kamat, The Journal of Physical Chemistry C 116.22 (2012) 11849 https://doi.org/10.1021/jp305026h
[3] D. Ziental, B. Czarczynska-Goslinska, D.T. Mlynarczyk, A. Glowacka-Sobotta, B. Stanisz, T. Goslinski, L. Sobotta, Nanomaterials 10.2 (2020) 387 https://doi.org/10.3390/nano10020387
[4] William Vallejo, Mauricio Meza, Fernando Durán, Carlos Diaz-Uribe, Cristian Quiñones, Elmar Schott, Xavier Zarate, Chemistry 7 (2025) 177 https://doi.org/10.3390/chemistry7060177
[5] Yujing Ma, Xiaobo Wang, Yudong Jia, Xintong Chen, Yujie Mao, Junjun Xu, Chemical Reviews 114.19 (2014) 9987 https://doi.org/10.1021/cr500008u
[6] Fernando G. Durán, Carlos Diaz-Uribe, Wilmar Vallejo, Alejandro Muñoz-Acevedo, Elmar Schott, Xavier Zarate, ACS Omega 8 (2023) 27284 https://doi.org/10.1021/acsomega.3c02657
[7] Andani Mkhohlakali, Te-Chang Jen, Kagiso Ledwaba, Sphamandla Mapukata, Hafeni M. Mabowa, Mothusi R. Letsoalo, Nchu Ntsasa, Juliana Tshilongo, Frontiers in Chemical Engineering 6 (2024) 1352283 https://doi.org/10.3389/fceng.2024.1352283
[8] Bijay Pant, Min Park, Soo-Jin Park, Coatings 9.10 (2019) 613 https://doi.org/10.3390/coatings9100613
[9] Ugo Bellè, Maria Rossi, Luca Bianchi, Alessandro Conti, Catalysts 13 (2023) 494 https://doi.org/10.3390/catal13030494
[10] Altaf A. Abdulwahid, Huda H. H. Al-Ani, Ali S. Mohammed, Inorganica Chimica Acta 501 (2020) 119268 https://doi.org/10.1016/j.ica.2019.119268
[11] Eka Widyastuti, Chien-Ting Chiu, Jiun-Ling Hsu, Yu-Chun Lee, Arabian Journal of Chemistry 16 (2023) 105010 https://doi.org/10.1016/j.arabjc.2023.105010
[12] W. Gibbs, M. Torris, Experimental and Theoretical NANOTECHNOLOGY 3 (2019) 103 https://doi.org/10.56053/3.1.103
[13] Kok-On Ong, Jun Cheong, Fah Heong, Experimental and Theoretical NANOTECHNOLOGY 4 (2020) 1 https://doi.org/10.56053/4.1.1
[14] Carmine Calabrese, Anja Maertens, Andrea Piras, Cristina Aprile, Luigi F. Liotta, Nanomaterials 13 (2023) 1928 https://doi.org/10.3390/nano13131928
[15] Chang Jia, Xiaoyan Zhang, Peng Yang, Applied Surface Science 430 (2018) 457 https://doi.org/10.1016/j.apsusc.2017.06.163

[16] Nirmala Geetha, Shanmugam Sivaranjani, Abdul Ayeshamariam, Mariadhas Valan Arasu, Nallusamy Punithavelan, Experimental and Theoretical NANOTECHNOLOGY 2 (2018) 139–150 https://doi.org/10.56053/2.3.139
[17] Maria A. Gatou, Anastasia Syrrakou, Niki Lagopati, Efthimia A. Pavlatou, Reactions 5 (2024) 135 https://doi.org/10.3390/reactions5010007
[18] Wei Jei, Jin Lim, Hung Hoa, Experimental and Theoretical NANOTECHNOLOGY 4 (2020) 47–58 https://doi.org/10.56053/4.3.47
[19] Rafik Sahnoun, Experimental and Theoretical NANOTECHNOLOGY 7 (2023) 78 https://doi.org/10.56053/7.2.78
[20] Muhammad Asjad, Muhammad Arshad, Naila A. Zafar, Muhammad A. Khan, Ahmed Iqbal, Ali Saleem, Abdulrahman Aldawsari, Materials Chemistry and Physics 265 (2021) 124416 https://doi.org/10.1016/j.matchemphys.2021.124416
[21] Ali Q. Tuama, Fadhil K. Farhan, Abothur Almohana, International Journal of Mechanical Engineering 7 (2022) 448.
[22] Thamer A. A. Hassan, Ali Q. Tuama, Ghaiath A. Fadhil, MINAR Congress of Pure, Applied and Technological Sciences 12 (2024) 239.
[23] Hayat Khan, Catalysts 15 (2025) 64 https://doi.org/10.3390/catal15010064
[24] Umar Samad, Muhammad Alam, Hisham Abdo, Ali Anis, Saad Al-Zahrani, Polymers 15 (2023) 3100 https://doi.org/10.3390/polym15143100
[25] Rida Rashid, Imran Shafiq, Muhammad R. H. S. Gilani, Muhammad Maaz, Parveen Akhter, Muhammad Hussain, Kwang-Eun Jeong, Eui-Eun Kwon, Seung Bae, Yong-Ki Park, Chemosphere 349 (2024) 140703 https://doi.org/10.1016/j.chemosphere.2023.140703
[26] Mehdi Rostami, Alireza Badiei, Mohammad R. Ganjali, Mohammad Rahimi-Nasrabadi, Majid Naddafi, Hossein Karimi-Maleh, Environmental Research 212 (2022) 113347 https://doi.org/10.1016/j.envres.2022.113347